JACS
JOURNAL OF THE AMERICAN CHEMICAL SOCIETY
Article
pubs.acs.org/JACS

# Coupled Oscillators for Tuning Fluorescence Properties of Squaraine Dyes

Christoph Lambert,* Thorsten Scherpf, Harald Ceymann, Alexander Schmiedel, and Marco Holzapfel

Institut für Organische Chemie, Universität Würzburg, Wilhelm Conrad Röntgen Research Center for Complex Material Systems, Center for Nanosystems Chemistry, Am Hubland, 97074 Würzburg, Germany

Supporting Information

**ABSTRACT:** Combining a squaraine (S) and a BODIPY (B) chromophore in a heterodimer (SB) and two heterotrimers (BSB and SBS) by alkyne bridges leads to the formation of coupled oscillators whose fluorescence properties are superior compared to the parent squaraine chromophore. The lowest energy absorption and emission properties of these superchromophores are mainly governed by the squaraine part and are shifted by more than 1000 $cm^{-1}$ to the red by excitonic interaction between the squaraine and the BODIPY dye. Employing polarization-dependent transient absorption and fluorescence upconversion measurements, we could prove that the lowest energy absorption in SB and BSB is caused by a single excitonic state but by two for SBS. Despite the spectral red-shift of their lowest absorption band, the fluorescence quantum yields increase for SB and BSB compared to the parent squaraine chromophore SQA. This is caused by intensity borrowing from the BODIPY states, which increases the squared transition moments of the lowest energy band dramatically by 29% for SB and 63% for BSB compared to SQA. Thereby, exciton coupling leads to a substantial enhancement of fluorescence quantum yield by 26% for SB and by 46% for BSB and shifts the emission from the red into the near-infrared. In this way, the BODIPY-squaraine conjugates combine the best properties of each class of dye. Thus, exciton coupling in heterodimers and -trimers is a valuable alternative to tuning fluorescence properties by, e.g., attaching substituents to chromophores.

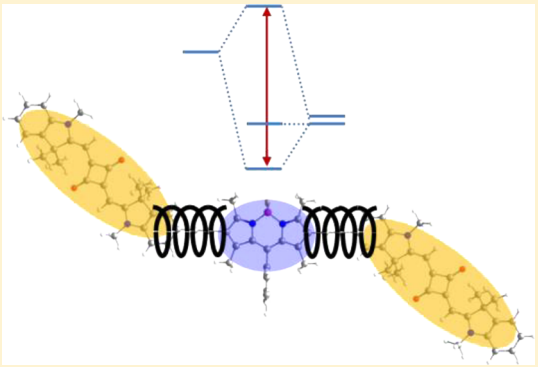

## INTRODUCTION

Fluorescence dyes emitting in the red or near-infrared with high quantum yield are highly sought after because of many technological[1−3] and medical applications.[4,5] In this context, tuning absorption and fluorescence energy characteristics of organic chromophores by attaching small substituents to a parent chromophore structure is a very popular but also limited method.[6,7] Often, broadening of absorption and/or decrease of fluorescence quantum yield are unwanted side effects.[8] Finding completely new chromophore archetypes requires extensive synthetic work and is also not easy to achieve.[9] Therefore, we follow an alternative route in which we combine different chromophores to form covalently bound superchromophores (SC).[10] In these SCs the transition moments of individual chromophores are coupled (exciton coupling) to produce new coupled oscillators whose resonance energy may deviate strongly from those of the individual chromophores.[11] Nature uses this concept in light harvesting employing huge complexes of chlorophyll molecules in the chromosomes of green bacteria. Artificial analogues are the J-aggregates of cyanine dyes whose enhanced coherent excitation and emission properties have been studied for decades.[12−16] This pretty old concept[17] has recently experienced a revival because the formation of J-aggregates may lead to what is nowadays frequently called "aggregation induced emission" (AIE).[18] In all these examples only one type of chromophore is employed; i.e., homoaggregates are considered. Much less is known about heterochromophore assemblies in which two or more *different* chromophores are incorporated, although this kind of dye assembly may open the chance to tune the SC properties considerably.[19,20]

In this paper we will investigate the photophysical properties of heterodimer and heterotrimer SCs built up from an indolenine squaraine dye and a BODIPY dye. The former were chosen as they display sharp and intense absorption bands in the red to near-infrared spectral region[21−24] and they are being used in numerous applications such as in biolabeling,[25−34] ion recognition,[35−39] nonlinear optics[40−47] and solar energy conversion.[48−72] BODIPY dyes are even more popular as fluorescence dyes absorbing in the green spectral region. They also show a relatively intense and narrow absorption band.[73−76] These are ideal conditions for investigating chromophore interactions in SCs because coupling induced shifts will easily be visible for strong and narrow absorption bands. In particular, we focus on the squaraine-BODIPY heterodimer SB, and the heterotrimers SBS and BSB (for their synthesis, see Supporting Information (SI)). In these SCs, the

Received: December 3, 2014
Published: March 4, 2015

ACS Publications © 2015 American Chemical Society



DOI: 10.1021/ja512338w
J. Am. Chem. Soc. 2015, 137, 3547−3557

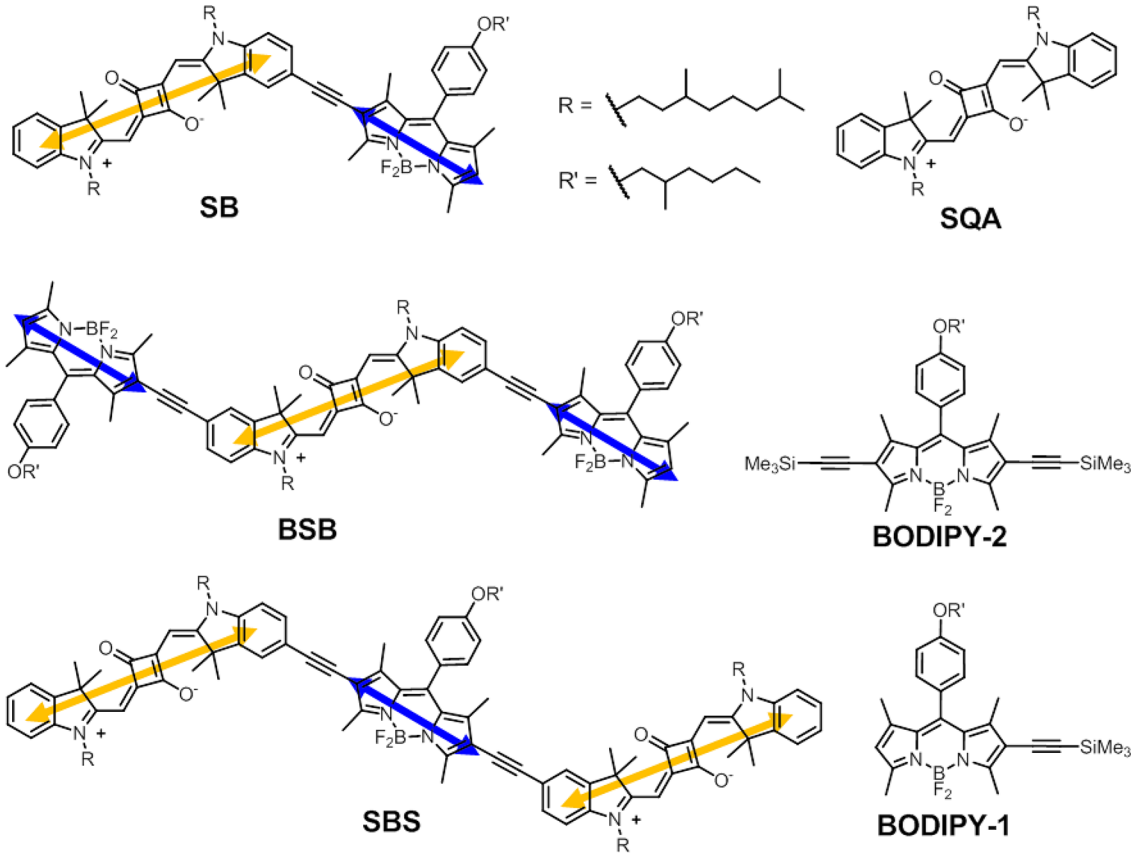


**Figure 1.** BODIPY and squaraine parent chromophores and heterodye conjugates along with their respective orientation of transition moments of the lowest energy localized states.

individual dyes were held together by triple bonds, which reduce flexibility and leads to fixed interchromophore distances although different conformers may result from rotation around the triple bonds. The steady-state and time-resolved optical properties will be investigated and compared to those of the parent chromophores SQA[10] and the BODIPY dyes BODIPY-1 and BODIPY-2[77] (see Figure 1).

## RESULTS AND DISCUSSION

The synthesis of the heterodimer SB and the two heterotrimers BSB and SBS was accomplished by copper-free Sonogashira reaction of appropriate bromine-substituted squaraines and alkyne-terminated BODIPY dyes (Scheme 1, see SI for details). The copper-free variant of Sonogashira reaction was used because of less formation of homocoupling products, which are difficult to remove from the target compounds.

The steady state absorption spectra of all SCs and their parent compounds in toluene are given in Figure 2a–c. The spectrum of SQA is typical of squaraine dyes and will serve as a reference. The spectrum is quite narrow (fwhm = 560 $cm^{-1}$) and has a weak vibronic shoulder to the higher energy side. The spectrum of the heterodimer SB displays a strong absorption at 15 000 $cm^{-1}$ similar to SQA but red-shifted by 500 $cm^{-1}$. A second, much weaker band at 19 000 $cm^{-1}$ is visible that is shifted by 100 $cm^{-1}$ compared to that of BODIPY-1, which we consider to be the most suitable dye for comparison. This drifting apart of electronic transitions is caused by exciton coupling of localized transition moments at the squaraine and BODIPY chromophore moieties, respectively. Figure 3 sketches the electronic situation for the head-to-tail arrangement of a homodimer that gives two excitonic states, split by twice the exciton coupling energy, $J$. The relative phase relations of the localized transition moments make the lowest exciton state being an allowed transition and the upper exciton state being forbidden. This scenario refers to the well-known J-type aggregate behavior.[10,15,78]

$$\delta E_{\mathrm{dimer}} = 2\sqrt{\Delta E^2 + J^2} \tag{1}$$

$$\mu^2 = \frac{3hc\varepsilon_0 \ln 10}{2000\pi^2 N} \frac{9n}{(n^2+2)^2} \int \frac{\varepsilon(\tilde{\nu})}{\tilde{\nu}}\, \mathrm{d}\tilde{\nu} \tag{2}$$

In heterodimers, the excitonic levels can be evaluated in the usual manner and are split by $\delta E_{\mathrm{dimer}}$ (eq 1), which is larger than $2J$ of the homodimer. In this equation, $2\Delta E$ is the energy difference between the diabatic (noninteracting) energy levels of the two chromophore units in the heterodimer. As zero energy, we take the midpoint between these diabatic levels. Because the transition moments are in general unequal for heterodimers, they do not cancel for the upper excitonic level in the head-to-tail arrangement, thus both states, the lower and the upper are allowed. This is exactly what we observe for SB. Interestingly, while the sum of the squared transition moments $\mu^2$ (calculated by integration of the spectra, see eq 2) for the squaraine and the BODIPY band are roughly that of the sum of the parent chromophores (189 $D^2$ vs 160 $D^2$), the one of the squaraine band in SB is larger (159 $D^2$ vs 123 $D^2$) and the one of the BODIPY band in SB is smaller (30.4 $D^2$ vs 36.5 $D^2$) than those of the respective parent compounds (see Table 1). This intensity borrowing is caused by the phase relations of the transition moments, which intensify the lower state on the


DOI: 10.1021/ja512338w
J. Am. Chem. Soc. 2015, 137, 3547–3557

**Scheme 1. Synthesis of SB, BSB and BSB by Copper-Free Sonogashira Reaction**

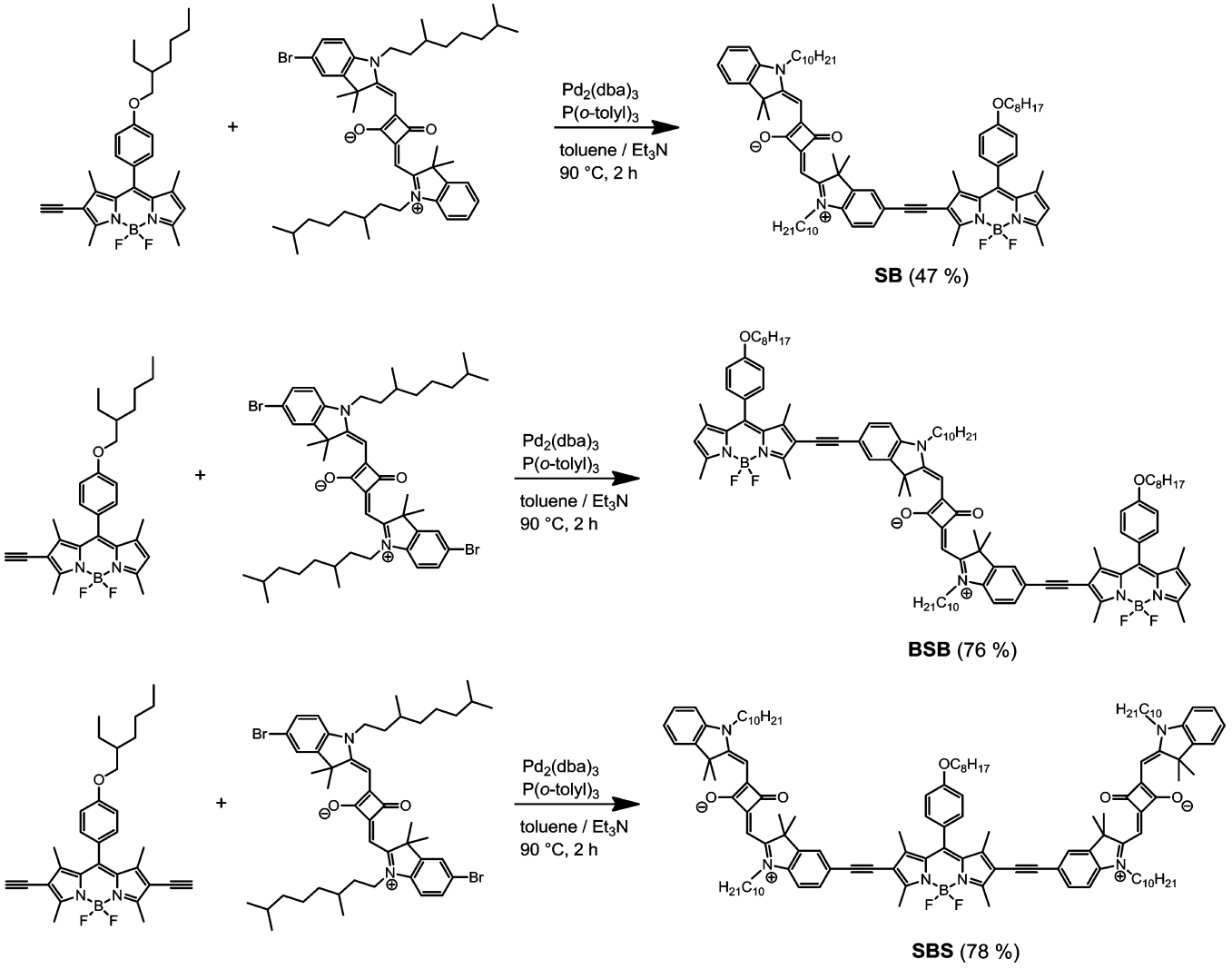


expense of the upper state in case of a head-to-tail arrangement.[79,80] The fact that SB shows an angle of ca. 120° between the chromophore long axes leads to some modification of intensity and orientation of resulting transition moments but we consider the head-to-tail model as qualitatively correct for our purposes. From the absorption maxima of SQA and BODIPY-1 we estimate $\Delta E = (\tilde{\nu}_{max}(\text{BODIPY-1}) - \tilde{\nu}_{max}(\text{SQA}))/2 = 1700\ \text{cm}^{-1}$ and with the experimental state splitting of SB = 4000 $\text{cm}^{-1}$ we evaluate an exciton coupling energy $|J| = 1050\ \text{cm}^{-1}$ by eq 1 (the coupling is negative for a head-to-tail arrangement).

In case of BSB the absorption spectra show an even more intense squaraine-type band at 14 400 $\text{cm}^{-1}$, which is strongly red-shifted compared to SQA by 1100 $\text{cm}^{-1}$, and a broad BODIPY-type band at 19 000 $\text{cm}^{-1}$. Again, the sum of squared transition moments of BSB is larger than that of the parent chromophores (271 $D^2$ vs 169 $D^2$) and the squaraine band is more intense (201 $D^2$ vs 123 $D^2$) and the BODIPY band is weaker (70.1 $D^2$ vs 2 × 36.5 $D^2$ = 73 $D^2$) than in the parent chromophores.

For BSB the exciton interaction matrix reads as in eq 3 where we adopt the nearest-neighbor approximation and neglect dispersion interactions between the chromophores in the ground state. Solving the secular determinant eq 3 yields the state diagram in Figure 3 with three exciton states and a state splitting of $\delta E_{trimer}$ (see eq 4) for the lower and upper state, which is in case of identical $\Delta E$ and $J$ values larger than that of the heterodimer. In the same way as for SB we estimate $|J| = 1100\ \text{cm}^{-1}$ by eq 4 for the exciton coupling energy in BSB, which is in excellent agreement with that in SB. Exciton coupling theory also predicts that the lowest exciton level carries most of the oscillator strength, the middle state is forbidden and the upper states carries less oscillator strength (for a compilation of all eigenvalues and eigenvectors, see SI).

At this point we would like to address an issue that has frequently led to misunderstandings: The exciton coupling energy is a quantity that enters in, e.g., eq 3, and which leads to a certain splitting/shifting of excited energy levels. With increasing energy difference $2\Delta E$ between the diabatic states, the influence of $J$ on this splitting becomes weaker but not the coupling energy itself, as is obvious when looking at eq 4. Therefore, the fact that many heterochromophore aggregates show only little energy displacements compared to their parent chromophores does not allow concluding on weak coupling, it may also be caused by a large $2\Delta E$. However, comparing eq 1 with eq 4 shows that the effect of $J$ on the splitting is larger for the trimer than for the dimer because of the $2J^2$ term in the root. For a heteropolymer this transforms into a $4J^2$ term.[10]



DOI: 10.1021/ja512338w
J. Am. Chem. Soc. 2015, 137, 3547−3557

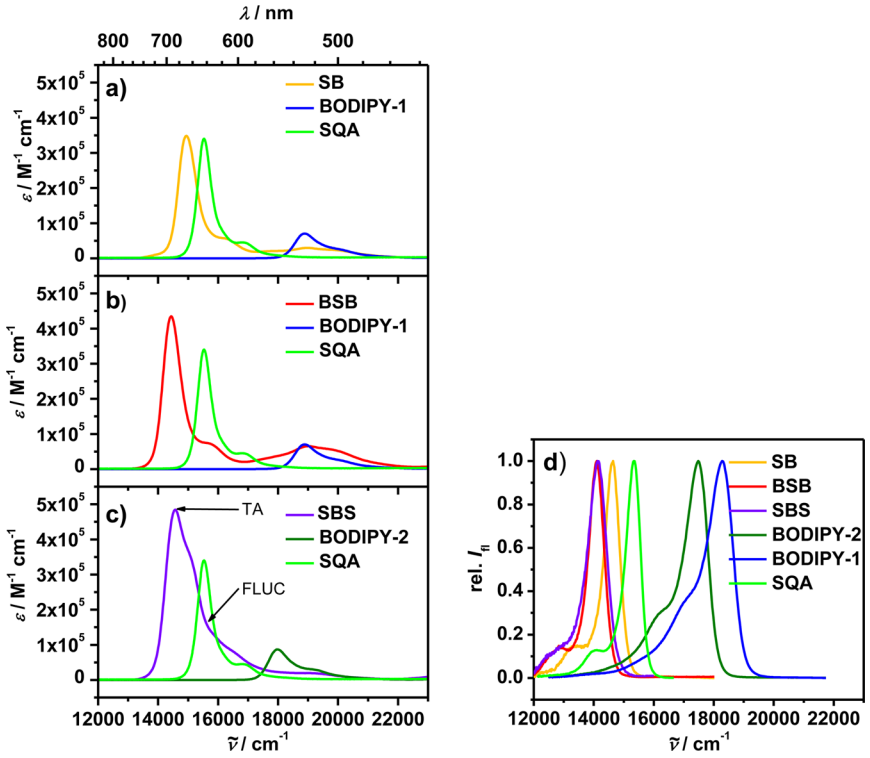


**Figure 2.** (a–c) Steady-state absorption spectra in toluene. In each panel the spectra of SB, BSB, and SBS are compared with their parent compounds SQA and BODIPY-1 or BODIPY-2, respectively. In panel (c) the pump wavenumbers for the FLUC and TA measurement are indicated. (d) Fluorescence spectra in toluene.

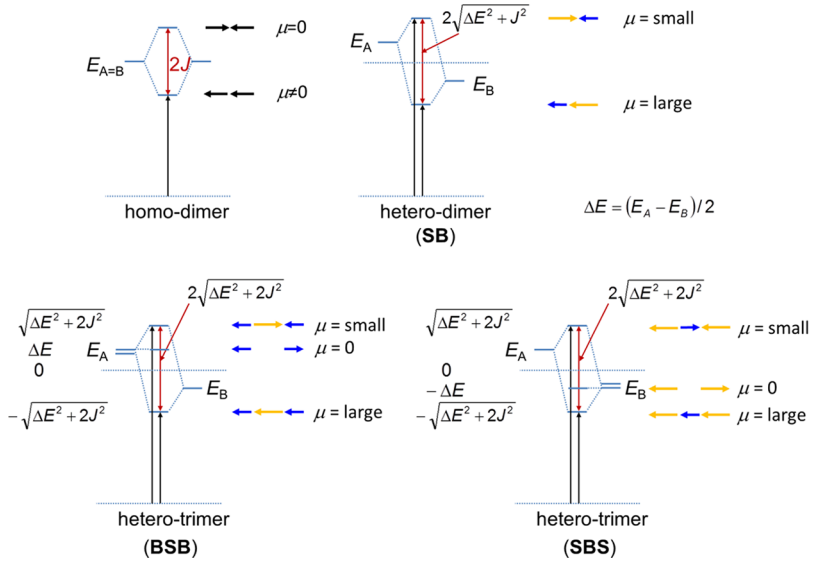


**Figure 3.** Exciton state diagram for dimers and trimers. The blue and orange vectors indicate the phase relations of transition moments and are not to scale.

$$\begin{vmatrix} \Delta E - \varepsilon & J & 0 \\ J & -\Delta E - \varepsilon & J \\ 0 & J & \Delta E - \varepsilon \end{vmatrix} = 0 \quad (3)$$

$$\delta E_{\text{trimer}} = 2\sqrt{\Delta E^2 + 2J^2} \quad (4)$$

In contrast to BSB and SB, which both show narrow squaraine bands similar to that of SQA, the heterotrimer SBS exhibits a much broader squaraine band at 14 600 $cm^{-1}$. However, the BODIPY band is much weaker and hardly visible at 19 000 $cm^{-1}$. For this reason we refrain from evaluating the separated squared transition moments and give that of the sum only, which is 339 $D^2$, compared to 291 $D^2$ for the sum of individual parent compounds. As reference compound for SBS we chose BODIPY-2 as this chromophore carries two acetylene groups that shift the absorption maximum by 900 $cm^{-1}$ to lower energy compared to BODIPY-1.

The exciton state diagram for SBS (Figure 3) is similar to that of BSB with the middle state now being closer to the lower


DOI: 10.1021/ja512338w
J. Am. Chem. Soc. 2015, 137, 3547–3557

**Table 1. Optical Data of Squaraine and BODIPY Dyes in Toluene at RT**

| | $\tilde{\nu}_{abs,1}$/cm$^{-1}$ ($\varepsilon$/M$^{-1}$ cm$^{-1}$) [fwhm/cm$^{-1}$][a] | $\mu_1^2$/D$^2$ [b] | $\tilde{\nu}_{abs,2}$/cm$^{-1}$ ($\varepsilon$/M$^{-1}$ cm$^{-1}$) [fwhm/cm$^{-1}$][c] | $\mu_2^2$/D$^2$ [d] | $\mu_1^2 + \mu_2^2$/D$^2$ | $\tilde{\nu}_{fl}$/cm$^{-1}$ [fwhm/cm$^{-1}$][e] | $\phi_f$[f] | $J$/cm$^{-1}$ [g] |
|---|---|---|---|---|---|---|---|---|
| SQA | 15 500 (340 000) [560] | 123 | | | 123 | 15 400 [590] | 0.57 ± 0.007 | |
| BODIPY-1 | | | 18 900 (70 600) [1090] | 36.5 | 36.5 | 18 300 [1090] | 0.78 ± 0.010 | |
| BODIPY-2 | | | 18 000 (86 900) [970] | 44.9 | 44.9 | 17 500 [920] | 0.92 ± 0.013 | |
| SB | 15 000 (348 000) [700] | 159 | 19 000 (29 600) | 30.4 | 189 | 14 600 [600] | 0.72 ± 0.014 | 1050 |
| BSB | 14 400 (435 000) [710] | 201 | 19 000 (65 200) | 70.1 | 271 | 14 100 [610] | 0.83 ± 0.025 | 1100 |
| SBS | 14 600 (484 000) | | 19 000 (19 600) | | 339 | 14 100 [750] | 0.53 ± 0.035 | 990[h] 1250[i] |

[a]Absorption energy (molar extinction coefficient) [full width at half-maximum] of the squaraine-type band. [b]Squared transition moment of the squaraine-type band. [c]Absorption energy (molar extinction coefficient) [full width at half-maximum] of the BODIPY-type band. [d]Squared transition moment of the BODIPY-type band. [e]Fluorescence wavenumber [full width at half-maximum]. [f]Absolute fluorescence quantum yield. [g]Exciton coupling energy. [h]Evaluated using BODIPY-2 as the reference chromophore. [i]Evaluated using BODIPY-1 as the reference chomophore.

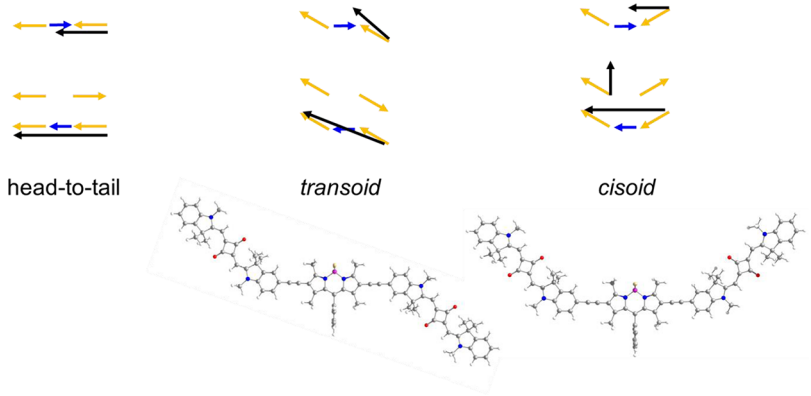


**Figure 4.** Vectorial representation of phase relations of transition moments of SBS for different orientations (DFT optimized geometries of model compounds without solubilizing alkyl chains at the bottom, see SI): orange vector = squaraine, blue vector = BODIPY, black vector = vector sum. The relative length of the orange and the blue vectors are arbitrary as they depend on the coefficients of eigenvectors (see SI).

state. As above, we evaluate $|J| = 990$ cm$^{-1}$, again in very good agreement with the coupling in SB and BSB. Using BODIPY-1 as reference compound would lead to $|J| = 1250$ cm$^{-1}$.

Compared to the BODIPY parent chromophores, attaching two trimethylsilylacetylene groups to SQA only leads to a 400 cm$^{-1}$ shift (15 100 cm$^{-1}$[81] vs 15 500 cm$^{-1}$ (SQA)). We stress that the choice of the proper reference chromophore is crucial for the evaluation of the electronic coupling, which thereby introduces a major source of error. The above evaluated coupling energies thus should be considered as a function of the choice of diabatic states (= noninteracting parent chromophores).

The broadness of the squaraine band in SBS might be caused by different conformers, which may adopt a *cisoid* and a *transoid* structure concerning the relative orientation of squaraine dyes to each other. This fact requires modifying the phase relations of transition moments as given in Figure 4. Now we have to take into account the ca. 120° angle between the chromophores (for DFT computed molecular structure, see SI), which leads to a nonvanishing vector sum of transition moments for the middle state in case of the *cisoid* arrangement of chromophores. This transition is now allowed and refers to the intense shoulder in the absorption spectra of SBS at ca. 15 000 cm$^{-1}$.

The steady-state fluorescence spectra (see Figure 2d) of all squaraine-containing compounds show very small Stokes shifts (on the order of 100−500 cm$^{-1}$) and similar band shapes as that of the parent squaraine SQA, which displays mirror image to its absorption spectrum. The fact that the fluorescence spectrum of SBS does not display mirror image to its absorption spectrum supports the assumption that the broad squaraine absorption of SBS stems from two different excitonic states as only the lowest one should lead to fluorescence. The fluorescence spectra of the BODIPY dyes are also mirror images of their respective absorption spectra. Comparison of all these spectra shows that the lowest excitonic states of the heterodimer and the heterotrimers have essentially squaraine character. As a consequence of exciton coupling, the fluorescence of these SCs is strongly red-shifted (800−1300 cm$^{-1}$) compared to that of SQA and extends into the NIR. Fluorescence quantum yields were determined for all dyes with


DOI: 10.1021/ja512338w
J. Am. Chem. Soc. 2015, 137, 3547−3557

**Table 2. Time-Resolved Optical Data of Squaraine and BODIPY Dyes in Toluene at RT**

| | $\tau_f$/ns (TCSPC)[a] | $k_f = \phi_f/\tau_f/s^{-1}$ [b] | $\tau_i$/ps ($a_i$) (FLUC)[c] | $\tau_i$/ps (TA)[d] | $\tau_a$/ps ($r(t=0)$) anisotropy (FLUC)[e] | $\tau_a$/ps ($r(t=0)$) anisotropy (TA)[f] |
|---|---|---|---|---|---|---|
| SQA | 1.7 | $3.35 \times 10^8$ | 0.31 (−0.091)<br>16 (−0.027)<br>1400 (1)<br>[16 900/15 300] | 1.0<br>740<br>1900<br>[15 500] | 200 (0.4)<br>[16 900/15 300] | 200 (0.36)<br>[15 500/14 200]<br>180 (0.35)<br>[15 500/15 400] |
| BODIPY-1 | 4.7 | | | | | |
| BODIPY-2 | 4.5 | | | | | |
| SB | 1.9 | $3.79 \times 10^8$ | 170 (0.115)<br>1900 (1)<br>[16 400/14 500] | 1.4<br>50<br>490<br>2000<br>[14 900] | 440 (0.36)<br>[16 400/14 500] | |
| BSB | 1.8 | $4.61 \times 10^8$ | 0.51 (−0.104)<br>35 (−0.176)<br>1500 (1)<br>[15 400/13 900]<br>0.70 (−0.070)<br>34 (−0.123)<br>1700 (1)<br>[19 000/[13 700] | 1.0<br>50<br>320<br>1800<br>[14 500] | 980 (0.38)<br>[15 400/13 900]<br>1090 (0.025)<br>[19 000/13 700] | |
| SBS | 1.3 | $4.08 \times 10^8$ | 0.29 (−0.246)<br>70 (−0.197)<br>450 (0.150)<br>1200 (1)<br>[15 600/14 000] | 0.13<br>5.0<br>88<br>1200<br>[14 600] | 960 (0.15)<br>[15 600/14 000] | 1400 (0.36)<br>[14 600/14 500] |

[a]Fluorescence lifetime measured TCSPC, excitation at 15 200 $cm^{-1}$ (squaraine dyes) and 23 900 $cm^{-1}$ (BODIPY dyes), emission at the emission maximum. [b]Radiative rate constant. [c]Fluorescence lifetime (amplitudes) [excitation/fluorescence wavenumber] measured by FLUC. [d]Globally fitted lifetimes of SADS measured by TA [pump wavenumber]. [e]Lifetime of anisotropy decay (initial anisotropy) [excitation/fluorescence wavenumber] measured by FLUC. [f]Lifetime of anisotropy decay (initial anisotropy) [excitation/probe wavenumber] measured by TA.

an integration sphere. The amazing point is that for both SB ($\phi_f$ = 0.72) and BSB ($\phi_f$ = 0.83) the fluorescence quantum yield increases compared to SQA ($\phi_f$ = 0.57) due to the interaction with the BODIPY dye. This contradicts the gap rule, which suggests increasing rates of nonradiative processes while going to lower fluorescence energies.[82,83] In contrast, the quantum yield of SBS is much smaller than that of SB and BSB and even SQA, which is likely caused by the allowed middle state in the *cisoid* conformer.

The BSB and SBS superchromophores behave also much differently from a recently described squaraine-fluorene-squaraine heterotrimer,[84] which displays very similar absorption and emission properties to its parent squaraine chromophore presumably because the excited state of the fluorene moiety is too high in energy and excitonic couplings exert only little changes of state energies. On the other hand, Therien et al. compared alkyne-connected Zn-porphyrin oligomers consisting of identical chromophores with oligomers of alternating slightly different Zn-porphyrins.[85,86] While impressive red-shifts of absorption and fluorescence were found for both series, the spectral width of the absorption band also increases strongly with the number of porphyrin units.

The above-described steady-state optical properties of SB, BSB, and SBS can quantitatively be understood by exciton coupling theory. In order to probe the influence of the excitonically coupled chromophores on the dynamic optical properties we performed time-resolved fluorescence and transient absorption experiments.

To cover and compare the whole temporal evolution of all chromophores by fluorescence spectroscopy, we measured the fluorescence decays of all chromophores by time-correlated single-photon counting (TCSPC, IRF ca. 200 ps) in toluene. From the results in Table 2 it is obvious that while the BODIPY dyes show monoexponential decays with lifetimes of ca. 4−5 ns the squaraine dyes have lifetimes of ca. 1.7−1.9 ns, with exception of SBS, which has a significantly reduced lifetime of 1.3 ns. Using these lifetimes and the fluorescence quantum yield we calculated the fluorescence rate $k_f = \phi_f/\tau_f$ (see Table 2), which is larger for SB and BSB compared to SQA and explains the effect of intensity borrowing on the basis of rate constants.

For the squaraine dyes better time resolution was obtained by fluorescence upconversion (FLUC) measurements with fs-time resolution (see Table 2 and SI). These measurements show multiexponential decays even for the SQA parent chromophore but the longest lifetime is in good agreement with the TCSPC results in all cases. For SQA, small negative amplitudes for the 0.31 and 16 ps component are indicative of dynamic changes of the fluorescence spectral band shape, which is probably caused by intramolecular vibrational relaxation (IVR) and vibrational cooling (VC)[87−89] because solvent relaxation effects are supposed to be small considering the nonpolar excited state and the nonpolar toluene.[90] Similar observations were made for BSB but not for SB, which shows only two decay components. In any case, the longest component dominates by far the decay to the ground state. We stress that for technical reasons it was not possible to excite


DOI: 10.1021/ja512338w
J. Am. Chem. Soc. 2015, 137, 3547−3557

the chromophores at the absorption maxima of the spectra and to measure the fluorescence decay at the maxima of the respective fluorescence spectra. This has to do with the excitation and emission wavenumber being very close and also close to the laser fundamental, which leads to stray-light artifacts even when using a type-II BBO crystal for sum-frequency generation in the FLUC experiments. The observed rise-time and decay-time components may then depend on the specific excitation/emission wavenumber combination. Therefore, we refrain from discussing the minor components in more detail.

In order to circumvent the above-mentioned problems we measured transient absorption (TA) pump−probe spectra where we excited the samples in toluene at the maximum of their absorption with 140 fs laser pulses and probed the spectral difference with a white-light continuum between 12 500 and 25 000 $cm^{-1}$ (400−800 nm).[90] The original chirp- and stray-light corrected data can be found in the SI. Here we focus on global target fits to the transient wavenumber × time map. In these target fits we assume a consecutive model (A→ B → C etc. and A → $S_0$, B → $S_0$ etc.) where all spectral components are associated with species and, thus, yield "species associated difference spectra" (SADS), which are given in Figure 5. Each component is also allowed to decay directly to the ground state. The efficiencies for each reaction pathway are given in the reaction scheme in Figure 5 and were determined under the assumption that all SADS at the maximum bleaching signal show the same optical density because they should possess the same extinction coefficient. In general the SADS consist of three contributions: (negative) ground state bleaching (GSB) signals where the steady-state spectra show prominent absorption bands; a (negative) stimulated emission (SE) signal where the steady-state spectra show fluorescence (intensity divided by $\tilde{\nu}^2$), and (positive) excited state absorption (ESA) to higher lying states.

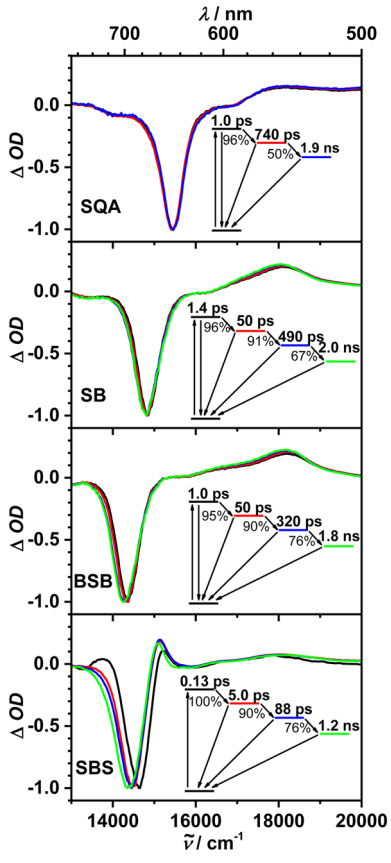


**Figure 5.** Species associated difference spectra of a global target fit to the transient absorption measurements in toluene. The inset gives state diagrams with the lifetimes and efficiencies of the corresponding excited states. $S_0$ and the initially pumped state are represented by black bars. The efficiency differences to 100% refer to the direct pathways to the ground state.

For SQA the SADS show strong bleaching associated with the strong $S_1$ ← $S_0$ GSB superimposed by SE $S_1$ → $S_0$ contribution to the low energy side. These two contributions merge to a strong negative signal with a minimum at 15 500 $cm^{-1}$. At 18 000−23 000 $cm^{-1}$ there is a broad and featureless ESA band (see SI). Between the first ($\tau$ = 1.0 ps) and the second ($\tau$ = 740 ps) SADS there is a slight red-shift of the SE flank of the 15 500 $cm^{-1}$ signal and between the second and the third ($\tau$ = 1.9 ns) SADS there is a slight blue-shift of both the GSB and the SE flanks. The shorter time constant (1.0 ps) is probably associated with an IVR process (see fluorescence upconversion results above). The slower process ($\tau$ = 740 ps) is difficult to assign to a specific process. One might speculate about vibrational cooling, which is so slow that in parallel relaxation to the ground state occurs. In fact this would be a continuous process and the representation by a single time constant is inadequate. Similarly long decay components were observed before for analogous squaraine dyes by other authors.[91,92] There, the hundred ps component was argued to be caused by an isomerization reaction. However, the long lifetime speaks against isomerization via a conical intersection as do the almost identical transient spectra for all three components (see Figure 5 and a magnification of the SADS in the SI). Furthermore, fluorescence anisotropy measurements (see below) also show no indication of an isomerization process.[93] Thus, an unspecified relaxation processes that goes along with little geometric/electronic changes appear to be the most likely explanation.

In SB the situation is similar to SQA, however, the global analysis procedure requires four components (see Table 2) whose SADS exhibit an increasing red-shift of the SE flank as does the low-energy side of the ESA at ca. 17 000−18 000 $cm^{-1}$. The SADS of BSB show a very similar scenario with very similar lifetimes of the components but with more pronounced red-shifts. Again, for SQA, SB and BSB the slowest component is in good agreement with the time-resolved emission measurements. The shorter components cannot be compared with the FLUC data because dynamic shifts of bands result in different lifetimes and amplitudes in a single color measurement as FLUC than in a globally fitted broad-band measurement such as the TA experiments. The dynamic properties of SB and BSB obviously are governed by the squaraine part of the SC.

Much in contrast to SQA, SB and BSB, the SADS of SBS show some additional features. These are, besides the superimposed GSB and SE at ca. 14 500 $cm^{-1}$, weak ESA signals at 13 800 and 15 200 $cm^{-1}$ for the component with the shortest lifetime ($\tau$ = 0.13 ps) and somewhat stronger ESA for all longer-lived components at the latter wavenumber. In addition, the successive red-shifts of the four SADS are even stronger than those in BSB and the associated lifetimes for the three shortest SADS are about 1 order of magnitude shorter compared to those of SB and BSB. This might be caused by the presence of cisoid and transoid conformers in SBS (see Figure 4) that are absent in BSB. The ESA at 15 200 $cm^{-1}$ may be


DOI: 10.1021/ja512338w
J. Am. Chem. Soc. 2015, 137, 3547−3557

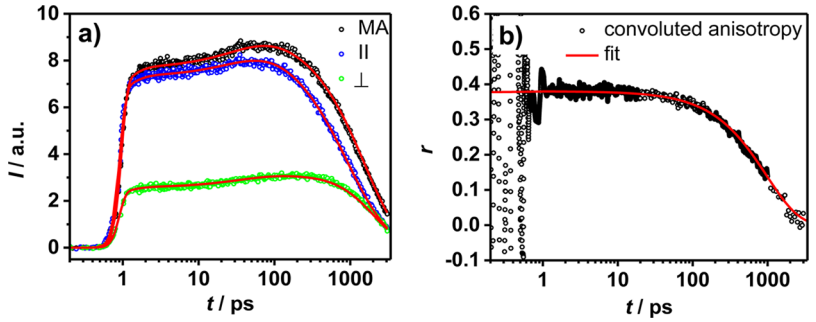


**Figure 6.** (a) Fluorescence upconversion measurements (circles) of BSB with pump pulse at magic angle (MA), parallel (||) and perpendicular (⊥) orientation relative to the gate pulse (pump at 15 400 $cm^{-1}$, fluorescence at 13 900 $cm^{-1}$). The MA data are not to scale to the parallel and perpendicular data. Global convoluted fit curves (red lines). (b) Experimental fluorescence anisotropy and convoluted anisotropy *r*.

caused by a two-exciton state, that is, transitions into a state where both squaraine chromophores are excited.[94] The more pronounced red-shift points toward stronger molecular reorientation processes in the excited state.

As indicated above, the deviations of the optical properties of SBS from, e.g., BSB may be traced back to excitation to the middle state being allowed caused by the presence of conformers. Such geometric changes should be visible in the time-resolved anisotropy of fluorescence, which is sensitive to changes of the orientation of the transition moment of the emitting state vs the transition moment of the primarily excited state.[95] Therefore, we determined the time-resolved fluorescence anisotropy $r(t)$ (see eq 5) by FLUC for all squaraine containing chromophores. In this equation, $\theta$ refers to the angle between the excitation and the emission transition moment. The anisotropy was determined by measuring the time-dependent fluorescence at parallel, perpendicular and magic angle orientation of the pump pulse relative to the gate pulse (see Figure 6). These time traces were deconvoluted by the instrument response (assumed to be Gaussian-shaped) and globally fitted, which yields the isotropic decay times and amplitudes and the anisotropic decay time together with its amplitude.[96] In all cases, $r(t)$ shows a monoexponential decay (Table 2) whose lifetime is related to the rotational diffusion and, thus reflect the increasing hydrodynamic radius of chromophores in the series $\tau_a$(SQA) = 200 ps, $\tau_a$(SB) = 440 ps, $\tau_a$(BSB) = 980 ps, and $\tau_a$(SBS) = 960 ps.[97]

$$r(t) = \frac{I_{\parallel}(t) - I_{\perp}(t)}{I_{\parallel}(t) + 2I_{\perp}(t)} = \frac{2}{5} \cdot \frac{3\cos^2\theta - 1}{2} \quad (5)$$

Even more interesting is the anisotropy (amplitude) at $t = 0$, which can be related to the angle $\theta$ between the excitation and the emission transition moment before rotational diffusion or other processes such as energy transfer or energy relaxation leads to a decay of anisotropy with time (see eq 5). The initial anisotropy $r(t = 0)$ is almost 0.4 for SQA, SB, and BSB (see Table 2) referring to 0° angle; that is, the transition moment for absorption and emission are parallel, which is what we expect for the emitting state being the same as the excited state. However, SBS shows $r(t = 0) = 0.15$, which refers to 40°. As stated above, because of technical reasons we excited the samples at the high energy flank of the squaraine band at 16 400 $cm^{-1}$ for SB, 15 400 $cm^{-1}$ for BSB and 15 600 $cm^{-1}$ for SBS. In case of SBS this means that we excited predominantly the middle exciton level of the *cisoid* conformer. Internal conversion to the lowest exciton state is a prerequisite to emit fluorescence. As sketched in Figure 4 the transition moment of the middle state and the lowest exciton state have an angle of ca. 90°, which theoretically refers to an initial anisotropy $r(t = 0) = -0.2$. In case of the *transoid* isomer we can only excite the lowest exciton state, which should result in $r(t = 0) = 0.4$. If we assume a mixture of *cisoid* and *transoid* conformers with, e.g., equal amounts this would result in an anisotropy of $(r(90°) + r(0°))/2 = (-0.2 + 0.4)/2 = 0.1$ in reasonable agreement with experiment.

In order to support the assumption that we excite a mixture of conformers of SBS we performed polarization dependent TA measurements. In general, unlike fluorescence measurements, where the anisotropy is always between −0.2 and +0.4, for TA measurements the anisotropy can adopt all values between −∞ and +∞ because several signals (GSB, SE, ESA) can contribute at a single wavenumber.[98] However, at the GSB/SE band of the squaraine dyes (around 14 000−16 000 $cm^{-1}$), there is hardly any ESA signal contribution. Because GSB of the lowest excited state and the ESA signal are expected to possess the same direction of transition moments this should simplify the analysis. This assumption is confirmed by measuring the TA anisotropy of SQA by pumping at 15 500 $cm^{-1}$ and probing at 14 200 $cm^{-1}$, which indeed gives $r(t = 0) = 0.36$ as expected for a lowest energy pumped and probed state with minimal overlap with other states. For SBS we pumped at 14 600 $cm^{-1}$, which is at the lowest exciton level and probed at 14 500 $cm^{-1}$ yielding $r(t = 0) = 0.36$. Again, this high anisotropy shows that we pumped and probed the identical lowest energy state. Thus, this TA experiment at 14 600 $cm^{-1}$ pump wavenumber together with the FLUC anisotropy measurement, which shows a much lower anisotropy at 15 600 $cm^{-1}$ pump wavenumber, proves that the squaraine absorption band between 14 000 and 17 000 $cm^{-1}$ of SBS consists of the lower *and* the middle excitonic states.

Finally it is instructive to see what happens if the BODIPY state of SB and BSB is excited at 18 900 $cm^{-1}$ (the BODIPY band of SBS is too weak for such an experiment). While the TA spectra (SADS) and their associated lifetimes are similar to the ones pumped at the maximum of the squaraine band (see SI), the initial anisotropy of the FLUC measurement of BSB is 0.025 ($\tau_a$(BSB) = 1090 ps in excellent agreement with the experiment at 15 400 $cm^{-1}$ pump wavenumber, see Table 2 and SI). This surprisingly low initial value indicates energy transfer from the upper excitonic state to the emitting lowest state being much faster than our time resolution (<200 fs).



DOI: 10.1021/ja512338w
J. Am. Chem. Soc. 2015, 137, 3547−3557

## CONCLUSIONS

Combination of two different chromophores, squaraine and BODIPY, in a heterodimer and two heterotrimers allowed tuning the superchomophore properties. The lowest energy absorption and emission properties are mainly governed by the squaraine part of the SCs, which can be shifted by more than 1000 $cm^{-1}$ to the red by the excitonic interaction with the BODIPY dye. The exciton coupling energy is ca. 1000 $cm^{-1}$ for all squaraine-containing SCs, which is substantial compared to, e.g., squaraine polymers with $|J| \sim 400-700$ $cm^{-1}$[10,49] but similar to thiophene-bridged squaraine dyes.[40] Employing polarization-dependent TA and FLUC measurements we could prove that the squaraine absorption in SB and BSB is caused by a single excitonic state but they are two for SBS. In this way, the dynamic properties of SBS differ from those of all other squaraine compounds in terms of dynamic Stokes shift, lifetimes and, most importantly, fluorescence quantum yield, which is decreased compared to SQA. For SB and BSB the situation is quite different: despite the spectral red-shift of the lowest absorption band, the fluorescence quantum yields increase for SB and BSB compared to SQA, which contradicts Siebrand's gap rule. This is caused by intensity borrowing from the BODIPY states, which increases the squared transition moments of the squaraine band dramatically by 29% for SB and 63% for BSB compared to SQA. In this way, exciton coupling can lead to a substantial enhancement of fluorescence quantum yield by 26% for SB and 46% for BSB and shift the emission from the red to the near-infrared while keeping the bandwidth almost constant. Thus, exciton coupling in heterochromophore systems represents an alternative way to tune and improve fluorescence properties of dyes provided that the excited state energies of the two chromophore units are not too far away. In conclusion, the here investigated superchomophores combine the best of two worlds, the high fluorescence quantum yield of BODIPY dyes with the low energy fluorescence of squaraine chromophores.

## EXPERIMENTAL SECTION

**Steady-State Absorption Spectroscopy.** All dyes were dissolved in toluene (Uvasol from Merck) and the UV/vis/NIR-absorption spectra were measured in 1 cm quartz cuvettes from Hellma using a Cary 5000 spectrometer. The pure solvent was used as reference.

**Femtosecond Transient-Absorption Spectroscopy.** The samples were dissolved in toluene (Uvasol from Merck), degassed for 30 min, filtered and stirred throughout the measurement. The experiments were performed in 2 mm fused silica cuvettes (Spectrocell Inc.) at RT and the optical density was adjusted to ca. 0.3 at the corresponding excitation wavenumber. The pump−probe measurements were performed with a Helios transient spectrometer from Ultrafast Systems and an amplified Ti:sapphire oscillator (Solstice) from Newport Spectra Physics (pulse length of 100 fs) with a repetition rate of 1 kHz and a fundamental wavenumber of 12 500 $cm^{-1}$ (800 nm). The output beam from the Solstice amplifier was split into two parts. A small part was focused onto a vertically oscillating $CaF_2$ crystal to generate a white light continuum between 11 900 $cm^{-1}$ (840 nm) and 25 000 $cm^{-1}$ (400 nm), which was polarized horizontally (the polarization was adjusted by using a wire grid (Thorlabs)) and used as the probe pulse. The main part was used to pump an optical parametric amplifier (TOPAS-C) from Light Conversion to generate the pump pulse with a pulse length of 140 fs at the corresponding excitation wavenumbers (SQA: 15 500 $cm^{-1}$, SB: 14 900 $cm^{-1}$, BSB: 14 500 $cm^{-1}$, SBS: 14 600 $cm^{-1}$). By means of a $\lambda/2$-plate and a wire grid (Thorlabs) the polarization axis of the pump pulse was set to 45° relative to that of the probe beam. With a second wire grid the probe beam was then adjusted to parallel, perpendicular and magic angle relative to the probe beam. This ensures that the sample was excited with the same intensity in the parallel and perpendicular measurements. The pump pulse (Ø ca. 0.5 mm) and probe pulse (Ø ca. 0.1 mm) met at ca. 6° vertical angle in the sample cuvette The probe light was measured by a spectrograph equipped with a CMOS sensor (Ultrafast Systems, Helios) in the range between 11 900 and 25 000 $cm^{-1}$ with an intrinsic resolution of 1.5 nm. Every second pump pulse was blocked by a mechanical chopper (working at 500 Hz) to measure $I$ and $I_0$. In order to compensate intensity fluctuations, a reference beam was split off and also detected with an identical spectrograph.

By means of a computer-controlled linear stage (retro reflector in double pass setup) the relative temporal delay between pump and probe pulse was varied in 20 fs steps from 0 fs to 4 ps and from 4 ps to 8 ns in logarithmic steps with a maximum step size of 200 ps. Steady state absorption spectra were recorded before and after the transient absorption experiment to exclude degradation of the sample. The raw data were corrected for stray light prior to data analysis of the difference spectra map (time × wavelength).

The maps recorded under magic angle conditions were analyzed with GLOTARAN[99,100] including the correction for the white light dispersion (chirp) and modeling the instrument response function and the coherent artifact. The anisotropic data were analyzed by a simultaneous reconvolution fit of the parallel, perpendicular and magic angle traces at selected wavelengths with a self-written implementation in MatLab. A detailed description of this procedure can be found in the literature.[101] Briefly, the measured signal intensity $I$ is the convolution of the instrument response IRF (taken as Gaussian shaped) with the product of the population decay function $S$ and respective anisotropy function, which depends on $r$.

$$\begin{bmatrix} I_{\parallel}(t) \\ I_{\perp}(t) \\ I_{MA}(t) \end{bmatrix} = \left( S(t) \begin{bmatrix} 1 + 2r(t) \\ 1 - r(t) \\ 1 \end{bmatrix} \right) \otimes \mathrm{IRF} \tag{6}$$

**Emission Spectroscopy.** Steady-state fluorescence measurements were performed with an Edinburgh Instruments FLS980 spectrometer. The compounds were dissolved in toluene (Uvasol from Merck) and purged with argon gas for 30 min prior to each measurement. Fluorescence quantum yields were measured with an integrating sphere and the FLS980 spectrometer applying the method of Bardeen et al.[102] to correct for self-absorption. Fluorescence lifetimes were determined by time-correlated single-photon counting (TCSPC) with the FLS980 spectrometer by exciting the samples with pulsed laser diodes at 15 200 $cm^{-1}$ (SQA, SB, BSB, SBS) or at 23 900 $cm^{-1}$ (BODIPY-1, BODIPY-2) under magic angle conditions and using a fast PMT detector (H10720) for fluorescence detection. Deconvolution of the data (4096 channels) was done by measuring the instrument response function with a scatterer (LUDOX).

**Femtosecond Fluorescence-Upconversion Spectroscopy.** We used a commercial fluorescence upconversion setup (Halcyone from Ultrafsat Systems). The laser system was the same as for the fs-TA-experiments. The output beam was again divided in two parts. One part seeded the optical parametric amplifier (TOPAS from Newport Spectra Physics) to generate the pump pulse with a pulse length of 140 fs and an excitation wavenumber of 16 900 $cm^{-1}$ for SQA, 16 400 $cm^{-1}$ for SB, 15 600 $cm^{-1}$ for SBS and 15 400 $cm^{-1}$ for BSB. The other part of the output beam was used as the gate pulse (12 500 $cm^{-1}$), which was delayed over a maximum of 3 ns in 20 fs steps from 0 fs to 4 ps and in logarithmic steps from 4 ps to 3 ns with a maximum step size of 80 ps with a computer-controlled linear stage. The samples were prepared as for the fs-TA-experiments in 2 mm fused silica cuvettes (Spectrocell Inc.) and were stirred during the experiment. The pump pulse was focused onto the cuvette and the fluorescence light was collected and focused on a 0.5 mm BBO type II crystal for frequency upconversion with the gate pulse whose focus was adjusted to lay ca. 10 mm behind the BBO crystal. All lenses in the setup had a focal length of 100 mm and a thickness of 1.85 mm. The upconverted light


DOI: 10.1021/ja512338w
J. Am. Chem. Soc. 2015, 137, 3547−3557

was focused on the entrance slit of a double monochromator and measured by a PMT detector. For polarization dependent measurements the pump beam was set to 45° by a $\lambda/2$ plate relative to the horizontally oriented gate beam. The polarization of both beams was purified by wire grids (Moxtek). In front of the cuvette, the pump beam was finally adjusted to parallel, perpendicular and magic angle relative to the gate beam with a wire grid for reasons already explained in the section above. The analyses of the anisotropic fluorescence upconversion data was done exactly as for the anisotropic transient absorption data.

## ■ ASSOCIATED CONTENT

### Supporting Information

Synthetic protocols, eigenvalues and eigenvectors of exciton coupling theory, raw data of time-resolved measurements. This material is available free of charge via the Internet at http://pubs.acs.org.

## ■ AUTHOR INFORMATION


### Corresponding Author

christoph.lambert@uni-wuerzburg.de


### Notes

The authors declare no competing financial interest.

## ■ ACKNOWLEDGMENTS

We thank the DFG for funding this work within the Research Group FOR 1809.

## ■ REFERENCES


(1) Stender, B.; Voelker, S. F.; Lambert, C.; Pflaum, J. *Adv. Mater.* **2013**, *25*, 2943.
(2) Tessler, N.; Medvedev, V.; Kazes, M.; Kan, S.; Banin, U. *Science* **2002**, *295*, 1506.
(3) Yao, L.; Zhang, S.; Wang, R.; Li, W.; Shen, F.; Yang, B.; Ma, Y. *Angew. Chem., Int. Ed.* **2014**, *53*, 2119.
(4) Guo, Z.; Park, S.; Yoon, J.; Shin, I. *Chem. Soc. Rev.* **2014**, *43*, 16.
(5) Pansare, V. J.; Hejazi, S.; Faenza, W. J.; Prud'homme, R. K. *Chem. Mater.* **2012**, *24*, 812.
(6) Mayerhöffer, U.; Fimmel, B.; Würthner, F. *Angew. Chem., Int. Ed.* **2012**, *51*, 164.
(7) Heckmann, A.; Dümmler, S.; Pauli, J.; Margraf, M.; Köhler, J.; Stich, D.; Lambert, C.; Fischer, I.; Resch-Genger, U. *J. Phys. Chem. C* **2009**, *113*, 20958.
(8) Völker, S. F.; Renz, M.; Kaupp, M.; Lambert, C. *Chem.—Eur. J.* **2011**, *17*, 14147.
(9) Müller, T. J. J.; Bunz, U. H. F. *Functional Organic Materials: Syntheses, Strategies and Applications*; Wiley-VCH: Weinheim, 2007.
(10) Völker, S. F.; Schmiedel, A.; Holzapfel, M.; Renziehausen, K.; Engel, V.; Lambert, C. *J. Phys. Chem. C* **2014**, *118*, 17467.
(11) Kuster, S.; Geiger, T. *Dyes Pigm.* **2015**, *113*, 110.
(12) Würthner, F.; Kaiser, T. E.; Saha-Moeller, C. R. *Angew. Chem., Int. Ed.* **2011**, *50*, 3376.
(13) Möbius, D. *Adv. Mater.* **1995**, *7*, 437.
(14) Kobayashi, T. *J-Aggregates*; World Scientific: Singapore, 1996.
(15) Van Amerongen, H.; Valkunas, L.; Van Grondelle, R. *Photosynthetic Excitations*; World Scientific: Singapore, 2000.
(16) Kirstein, S.; Daehne, S. *Int. J. Photoenergy* **2006**, *2006*, 1.
(17) Scheibe, G. *Kolloid-Z.* **1938**, *82*, 1.
(18) Hong, Y.; Lam, J. W. Y.; Tang, B. Z. *Chem. Soc. Rev.* **2011**, *40*, 5361.
(19) Czikkely, V.; Dreizler, G.; Foersterling, H. D.; Kuhn, H.; Sondermann, J.; Tillmann, P.; Wiegand, J. *Z. Naturforsch., A: Astrophys., Phys. Phys. Chem.* **1969**, *24*, 1821.
(20) Kiprianov, A. I. *Russ. Chem. Rev.* **1971**, *40*, 594.
(21) Ajayaghosh, A. *Acc. Chem. Res.* **2005**, *38*, 449.
(22) Beverina, L.; Salice, P. *Eur. J. Org. Chem.* **2010**, 1207.
(23) Sreejith, S.; Carol, P.; Chithra, P.; Ajayaghosh, A. *J. Mater. Chem.* **2008**, *18*, 264.
(24) Yagi, S.; Nakazumi, H. *Top. Heterocycl. Chem.* **2008**, *14*, 133.
(25) Volkova, K. D.; Kovalska, V. B.; Tatarets, A. L.; Patsenker, L. D.; Kryvorotenko, D. V.; Yarmoluk, S. M. *Dyes Pigm.* **2006**, *72*, 285.
(26) Tatarets, A. L.; Fedyunyayeva, I. A.; Dyubko, T. S.; Povrozin, Y. A.; Doroshenko, A. O.; Terpetschnig, E. A.; Patsenker, L. D. *Anal. Chim. Acta* **2006**, *570*, 214.
(27) Terpetschnig, E.; Szmacinski, H.; Ozinskas, A.; Lakowicz, J. R. *Anal. Biochem.* **1994**, *217*, 197.
(28) Thomas, J.; Sherman, D. B.; Amiss, T. J.; Andaluz, S. A.; Pitner, J. B. *Bioconjugate Chem.* **2007**, *18*, 1841.
(29) Renard, B.-L.; Aubert, Y.; Asseline, U. *Tetrahedron Lett.* **2009**, *50*, 1897.
(30) Gao, F.-P.; Lin, Y.-X.; Li, L.-L.; Liu, Y.; Mayerhöffer, U.; Spenst, P.; Su, J.-G.; Li, J.-Y.; Würthner, F.; Wang, H. *Biomaterials* **2014**, *35*, 1004.
(31) Terpetschnig, E.; Szmacinski, H.; Lakowicz, J. R. *Anal. Chim. Acta* **1993**, *282*, 633.
(32) Arunkumar, E.; Fu, N.; Smith, B. D. *Chem.—Eur. J.* **2006**, *12*, 4684.
(33) Gassensmith, J. J.; Arunkumar, E.; Barr, L.; Baumes, J. M.; DiVittorio, K. M.; Johnson, J. R.; Noll, B. C.; Smith, B. D. *J. Am. Chem. Soc.* **2007**, *129*, 15054.
(34) Xiang, Z.; Nesterov, E. E.; Skoch, J.; Lin, T.; Hyman, B. T.; Swager, T. M.; Bacskai, B. J.; Reeves, S. A. *J. Histochem. Cytochem.* **2005**, *53*, 1511.
(35) Ros-Lis, J. V.; Martinez-Manez, R.; Sancenon, F.; Soto, J.; Spieles, M.; Rurack, K. *Chem.—Eur. J.* **2008**, *14*, 10101.
(36) Ros-Lis, J. V.; Martinez-Manez, R.; Soto, J. *Chem. Commun.* **2002**, 2248.
(37) Ajayaghosh, A.; Arunkumar, E.; Daub, J. *Angew. Chem., Int. Ed.* **2002**, *41*, 1766.
(38) Radaram, B.; Mako, T.; Levine, M. *Dalton Trans.* **2013**, *42*, 16276.
(39) Ananda Rao, B.; Kim, H.; Son, Y.-A. *Sens. Actuators, B* **2013**, *188*, 847.
(40) Scherer, D.; Dörfler, R.; Feldner, A.; Vogtmann, T.; Schwoerer, M.; Lawrentz, U.; Grahn, W.; Lambert, C. *Chem. Phys.* **2002**, *279*, 179.
(41) Odom, S. A.; Webster, S.; Padilha, L. A.; Peceli, D.; Hu, H.; Nootz, G.; Chung, S. J.; Ohira, S.; Matichak, J. D.; Przhonska, O. V.; Kachkovski, A. D.; Barlow, S.; Bredas, J. L.; Anderson, H. L.; Hagan, D. J.; Van Stryland, E. W.; Marder, S. R. *J. Am. Chem. Soc.* **2009**, *131*, 7510.
(42) Ohira, S.; Rudra, I.; Schmidt, K.; Barlow, S.; Chung, S.-J.; Zhang, Q.; Matichak, J.; Marder, S. R.; Brédas, J.-L. *Chem.—Eur. J.* **2008**, *14*, 11082.
(43) Toro, C.; De Boni, L.; Yao, S.; Ritchie, J. P.; Masunov, A. E.; Belfield, K. D.; Hernandez, F. E. *J. Chem. Phys.* **2009**, *130*, 214504/1.
(44) Webster, S.; Fu, J.; Padilha, L. A.; Przhonska, O. V.; Hagan, D. J.; Van Stryland, E. W.; Bondar, M. V.; Slominsky, Y. L.; Kachkovski, A. D. *Chem. Phys.* **2008**, *348*, 143.
(45) Webster, S.; Odom, S. A.; Padilha, L. A.; Przhonska, O. V.; Peceli, D.; Hu, H.; Nootz, G.; Kachkovski, A. D.; Matichak, J.; Barlow, S.; Anderson, H. L.; Marder, S. R.; Hagan, D. J.; Van Stryland, E. W. *J. Phys. Chem. B* **2009**, *113*, 14854.
(46) Webster, S.; Peceli, D.; Hu, H.; Padilha, L. A.; Przhonska, O. V.; Masunov, A. E.; Gerasov, A. O.; Kachkovski, A. D.; Slominsky, Y. L.; Tolmachev, A. I.; Kurdyukov, V. V.; Viniychuk, O. O.; Barrasso, E.; Lepkowicz, R.; Hagan, D. J.; Van Stryland, E. W. *J. Phys. Chem. Lett.* **2010**, *1*, 2354.
(47) Belfield, K. D.; Bondar, M. V.; Haniff, H. S.; Mikhailov, I. A.; Luchita, G.; Przhonska, O. V. *ChemPhysChem* **2013**, *14*, 3532.
(48) Silvestri, F.; Irwin, M. D.; Beverina, L.; Facchetti, A.; Pagani, G. A.; Marks, T. J. *J. Am. Chem. Soc.* **2008**, *130*, 17640.
(49) Völker, S. F.; Uemura, S.; Limpinsel, M.; Mingebach, M.; Deibel, C.; Dyakonov, V.; Lambert, C. *Macromol. Chem. Phys.* **2010**, *211*, 1098.
(50) Merritt, V. Y.; Hovel, H. J. *Appl. Phys. Lett.* **1976**, *29*, 414.




DOI: 10.1021/ja512338w
J. Am. Chem. Soc. 2015, 137, 3547−3557

(51) Morel, D. L.; Ghosh, A. K.; Feng, T.; Stogryn, E. L.; Purwin, P. E.; Shaw, R. F.; Fishman, C. *Appl. Phys. Lett.* **1978**, *32*, 495.
(52) Wang, S.; Mayo, E. I.; Perez, M. D.; Griffe, L.; Wei, G.; Djurovich, P. I.; Forrest, S. R.; Thompson, M. E. *Appl. Phys. Lett.* **2009**, *94*, 233304.
(53) Mayerhöffer, U.; Deing, K.; Gruss, K.; Braunschweig, H.; Meerholz, K.; Würthner, F. *Angew. Chem., Int. Ed.* **2009**, *48*, 8776.
(54) Fan, B.; Maniglio, Y.; Simeunovic, M.; Kuster, S.; Geiger, T.; Hany, R.; Nuesch, F. *Int. J. Photoenergy* **2009**, 1.
(55) Wei, G.; Wang, S.; Renshaw, K.; Thompson, M. E.; Forrest, S. R. *ACS Nano* **2010**, *4*, 1927.
(56) Wei, G.; Lunt, R. R.; Sun, K.; Wang, S.; Thompson, M. E.; Forrest, S. R. *Nano Lett.* **2010**, *10*, 3555.
(57) Beverina, L.; Drees, M.; Facchetti, A.; Salamone, M.; Ruffo, R.; Pagani, G. A. *Eur. J. Org. Chem.* **2011**, *2011*, 5555.
(58) Wei, G.-D.; Xiao, X.; Wang, S.-Y.; Zimmerman, J. D.; Sun, K.; Diev, V. V.; Thompson, M. E.; Forrest, S. R. *Nano Lett.* **2011**, *11*, 4261.
(59) Wang, S.; Hall, L.; Diev, V. V.; Haiges, R.; Wei, G.; Xiao, X.; Djurovich, P. I.; Forrest, S. R.; Thompson, M. E. *Chem. Mater.* **2011**, *23*, 4789.
(60) Wei, G.; Xiao, X.; Wang, S.; Sun, K.; Bergemann, K. J.; Thompson, M. E.; Forrest, S. R. *ACS Nano* **2012**, *6*, 972.
(61) Chen, C.-H.; Cheng, W.-T.; Tsai, M.-L.; Huang, K.-T. *Ind. Eng. Chem. Res.* **2012**, *51*, 3630.
(62) Xiao, X.; Wei, G.; Wang, S.; Zimmerman, J. D.; Renshaw, C. K.; Thompson, M. E.; Forrest, S. R. *Adv. Mater.* **2012**, *24*, 1956.
(63) Deing, K. C.; Mayerhöffer, U.; Würthner, F.; Meerholz, K. *Phys. Chem. Chem. Phys.* **2012**, *14*, 8328.
(64) Kylberg, W.; Zhang, Y.; Aebersold, A.; Araujo de Castro, F.; Geiger, T.; Heier, J.; Kuster, S.; Ma, C.-Q.; Bauerle, P.; Nuesch, F.; Tisserant, J.-N.; Hany, R. *Org. Electron.* **2012**, *13*, 1204.
(65) Maeda, T.; Tsukamoto, T.; Seto, A.; Yagi, S.; Nakazumi, H. *Macromol. Chem. Phys.* **2012**, *213*, 2590.
(66) Bagnis, D.; Beverina, L.; Huang, H.; Silvestri, F.; Yao, Y.; Yan, H.; Pagani, G. A.; Marks, T. J.; Facchetti, A. *J. Am. Chem. Soc.* **2010**, *132*, 4074.
(67) Choi, H.; Kamat, P. V. *J. Phys. Chem. Lett.* **2013**, *4*, 3983.
(68) Maeda, T.; Arikawa, S.; Nakao, H.; Yagi, S.; Nakazumi, H. *New J. Chem.* **2013**, *37*, 701.
(69) Maeda, T.; Hamamura, Y.; Miyanaga, K.; Shima, N.; Yagi, S.; Nakazumi, H. *Org. Lett.* **2011**, *13*, 5994.
(70) Maeda, T.; Nakao, H.; Kito, H.; Ichinose, H.; Yagi, S.; Nakazumi, H. *Dyes Pigm.* **2011**, *90*, 275.
(71) Maeda, T.; Shima, N.; Tsukamoto, T.; Yagi, S.; Nakazumi, H. *Synth. Met.* **2011**, *161*, 2481.
(72) Jiang, J.-Q.; Sun, C.-L.; Shi, Z.-F.; Zhang, H.-L. *RSC Adv.* **2014**, *4*, 32987.
(73) Bessette, A.; Hanan, G. S. *Chem. Soc. Rev.* **2014**, *43*, 3342.
(74) Ulrich, G.; Ziessel, R.; Harriman, A. *Angew. Chem., Int. Ed.* **2008**, *47*, 1184.
(75) Boens, N.; Leen, V.; Dehaen, W. *Chem. Soc. Rev.* **2012**, *41*, 1130.
(76) Loudet, A.; Burgess, K. *Chem. Rev.* **2007**, *107*, 4891.
(77) Popere, B. C.; Della Pelle, A. M.; Thayumanavan, S. *Macromolecules* **2011**, *44*, 4767.
(78) McRae, E. G.; Kasha, M. *Phys. Processes Radiat. Biol., Proc. Int. Symp.* **1964**, 23.
(79) Guelen, D. *Photosynth. Res.* **2006**, *87*, 205.
(80) Shibata, Y.; Tateishi, S.; Nakabayashi, S.; Itoh, S.; Tamiaki, H. *Biochemistry* **2010**, *49*, 7504.
(81) Chen, J.; Winter, R. F. *Chem.—Eur. J.* **2012**, *18*, 10733.
(82) Siebrand, W. *J. Chem. Phys.* **1967**, *46*, 440.
(83) Siebrand, W. *J. Chem. Phys.* **1967**, *47*, 2411.
(84) Moreshead, W. V.; Przhonska, O. V.; Bondar, M. V.; Kachkovski, A. D.; Nayyar, I. H.; Masunov, A. E.; Woodward, A. W.; Belfield, K. D. *J. Phys. Chem. C* **2013**, *117*, 23133.
(85) Duncan, T. V.; Susumu, K.; Sinks, L. E.; Therien, M. J. *J. Am. Chem. Soc.* **2006**, *128*, 9000.
(86) Susumu, K.; Therien, M. J. *J. Am. Chem. Soc.* **2002**, *124*, 8550.
(87) Glasbeek, M.; Zhang, H. *Chem. Rev.* **2004**, *104*, 1929.
(88) Elsaesser, T.; Kaiser, W. *Annu. Rev. Phys. Chem.* **1991**, *42*, 83.
(89) Pigliucci, A.; Duvanel, G.; Daku, L. M. L.; Vauthey, E. *J. Phys. Chem. A* **2007**, *111*, 6135.
(90) Reynolds, L.; Gardecki, J. A.; Frankland, S. J. V.; Horng, M. L.; Maroncelli, M. *J. Phys. Chem.* **1996**, *100*, 10337.
(91) de, M. G.; Marchena, M.; Zitnan, M.; Pandey, S. S.; Hayase, S.; Douhal, A. *Phys. Chem. Chem. Phys.* **2012**, *14*, 1796.
(92) Gude, C.; Rettig, W. *J. Phys. Chem. A* **2000**, *104*, 8050.
(93) For none of the squaraine dyes do we have any indication for the presence of different isomers/conformers in solution by, e.g., NMR spectroscopy. While rotation about the triple bond should be faster than the NMR time scale and, thus, be invisible, isomerization within the squaraine dyes around the double bonds should be slow and visible as two sets of NMR signals.
(94) Knoester, J. *Proc. Int. Sch. Phys. "Enrico Fermi"* **2002**, *149*, 149.
(95) Vogel, S. S.; Thaler, C.; Blank, P. S.; Koushik, S. V. In *FLIM Microscopy in Biology and Medicine*; Periasamy, A., Clegg, R. M., Eds.; Chapman and Hall/CRC Press: Boca Raton, FL, 2009.
(96) Cross, A. J.; Fleming, G. R. *Biophys. J.* **1984**, *46*, 45.
(97) Fleming, G. R. In *Chemical Applications of Ultrafast Spectroscopy*; Oxford University Press: Oxford, U.K., 1986.
(98) Jonas, D. M.; Lang, M. J.; Nagasawa, Y.; Joo, T.; Fleming, G. R. *J. Phys. Chem.* **1996**, *100*, 12660.
(99) Van Stokkum, I. H. M.; Larsen, D. S.; Van Grondelle, R. *Biochim. Biophys. Acta, Bioenerg.* **2004**, *1657*, 82.
(100) Snellenburg, J. J.; Laptenok, S. P.; Seger, R.; Mullen, K. M.; Stokkum, I. H. M. v. *J. Stat. Software* **2012**, *49*, 1.
(101) Steeger, M. Ph.D. Thesis, University of Würzburg, 2014.
(102) Ahn, T.-S.; Al-Kaysi, R. O.; Muller, A. M.; Wentz, K. M.; Bardeen, C. J. *Rev. Sci. Instrum.* **2007**, *78*, 086105.


DOI: 10.1021/ja512338w
*J. Am. Chem. Soc.* 2015, 137, 3547−3557